Magnetic properties of rare-earth metal tritellurides $R\mathrm{Te}_3$ (R=Ce,Pr,Nd,Gd,Dy)

Yuji Iyeiri, Teppei Okumura, Chishiro Michioka, and Kazuya Suzuki
Graduate School of Environment and Information Sciences, Yokohama National University, Hodogaya-ku, Yokohama 240-8501, Japan
(Received 23 October 2002; published 22 April 2003)

The magnetic properties of $R\mathrm{Te}_3$ (R=Ce, Pr, Nd, Gd, Dy), which has a structure consisting of the alternate stacking of one RTe layer and two Te layers, were investigated using magnetization and electrical resistivity measurements. The magnetic transition temperatures were found at 3.0 K for R=Ce, 3.2 K for Nd, 11.5 K for Gd, and 4.5 K for Dy, respectively, and the Pr compound showed van Vleck paramagnetism. The ordered magnetic moment of $R\mathrm{Te}_3$ lies within the layer. In contrast, the ordered magnetic moments of $R\mathrm{Te}_2$, having alternate stacking of one RTe and one Te layer, point to the layer-stacking direction, although the point symmetry at the R site and the coordination of the Te atoms to the R atoms are almost the same. The difference of the magnetic anisotropy in $R\mathrm{Te}_2$ and $R\mathrm{Te}_3$ was discussed in terms of the effective charge of the Te atoms in the Te layer with an electron charge transferred from the RTe layer. We propose magnetic compounds designed by charge introduction based on this result.

DOI: 10.1103/PhysRevB.67.144417 PACS number(s): 75.30.Gw, 75.25.+z, 71.27.+a

I. INTRODUCTION

When attempting to synthesize the compounds that have important magnetic properties or phenomena, a ''layered structure'' is one of the most important keys to be considered, since in some layered compounds the magnetic and electrical properties can be designed and controlled in each unit of the atomic layer. Here, we report a series of compounds with the magnetic anisotropy controlled by the introduction of an electric charge to the target atomic layer.

The rare-earth metal polytellurides $R\mathrm{Te}_2$ and $R\mathrm{Te}_3$ crystallize in the anti-Cu_2Sb and the $NdTe_3$ structure, respectively.[1–3] They have a common basic crystal structure consisting of the alternate layer stacking of the tetragonal Te layer, and RTe layer as shown in Fig. 1. The RTe layer is formed from the distorted two-layer slice of cubic RTe with the NaCl-type structure. This two-layer unit of the rare-earth chalcogenide is known in so-called ''misfit layer compounds'' $(RX)_x(TX_2)_y$, where X=S and Se, T=Ti, V, Cr, Nb, and Ta, x=1.13–1.23 being the irrational number due to the lattice mistfit between RX and TX_2, and y=1–3.[4,5] It is known in the compounds that the TX_2 layer carries electrical conduction, while the RX layer becomes insulating after the charge transfer to the TX_2 layer. Since the magnetic RX layer and the conducting TX_2 layer are well separated in space, the dominant magnetic interaction among the magnetic R ions is not the Ruderman-kittel-kasuya-Yosida (RKKY) interaction, but direct exchange or superexchange interaction. This is also the case for $R\mathrm{Te}_2$ or $R\mathrm{Te}_3$. The electronic structure is well described in terms of the rigid-band scheme with one-electron transfer from the RTe layer to the Te layer. Kikuchi showed by a first-principles calculation with the DV-$X\alpha$ method for $LaTe_2$ that the energy gap between the conduction and valence bands of the $(La^{3+}Te^{2-})$ unit is ca. 4 eV, while the conduction band of the Te^{1-} layer lies in the gap.[6] Since the conduction band of the Te layer is halffilled, the electronic properties are expected to be metallic, but are actually a poorly conducting semimetal. As the $(2\times1\times1)$ superstructure reflection is observed in the electron diffraction,[7] the zone holding of the first Brillouin zone by the superstructure makes a very small overlapping of the conduction band at the Fermi level. However, the origin of the superstructure, whether the electronic one (formation of the charge-density waves[7]) or the dimerization of the Te atoms due to the difference in the in-plane lattice constant of the RTe layer and the Te layer,[8] is still under discussion.

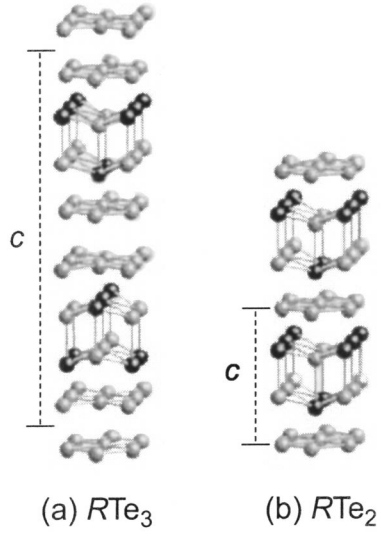

FIG. 1. Crystal structures of (a) $R\mathrm{Te}_3$ and (b) $R\mathrm{Te}_2$. Black and gray circles denote the R and Te atoms, respectively.

In contrast, a good metallic behavior was reported on $SmTe_3$.[9] An electron-diffraction study by DiMasi *et al.* showed that all the rare-earth tritellurides $R\mathrm{Te}_3$ form an incommensurate superstructure close to $(4\times1\times1)$.[10] The charge transfer from the RTe layer to the two Te layers makes an effective ionic state of $(\mathrm{Te}_2)^-$ and a quarter-filled conduction band in the Te layer. Then the differences in the superstructure formation and the electron density in the Te layer between $R\mathrm{Te}_2$ and $R\mathrm{Te}_3$ give a significant difference in the conducting properties.

The physical properties of $R\mathrm{Te}_2$ were first reported for

TABLE I. Physical parameters of $R\mathrm{Te}_3$. Q is the distortion wave vector detected from the Laue photograph. ρ_{rt} and $\rho_{1.5\,\mathrm{K}}$ are the resistivities at room temperature and 1.5 K, respectively, and RRR is the residual resistivity ratio. The effective magnetic moments and the Weiss temperatures are estimated from the Curie-Weiss fitting above 200 K. $T_{(\chi)\mathrm{anom}}$, the temperature at which $d\chi/dT$ is maximum; $T_{(\rho)\mathrm{anom}}$, the temperature at which the anomaly due to the magnetic transition appears.

R	Q Q/a^*	ρ_{rt} ($\mu\Omega$ cm)	$\rho_{1.5\,\mathrm{K}}$ ($\mu\Omega$ cm)	RRR $\rho_{rt}/\rho_{1.5\,\mathrm{K}}$	$T_{(\rho)\mathrm{anom}}$ (K)	μ_{eff} (μ_B)	θ (K)	$T_{(\chi)\mathrm{anom}}$ (K)
La ($\|a$)	0.272	111	0.52	213	-		Pauli paramagnetism	
Ce ($\|a$)	0.277	180	4.01	44.9	1.3, 3.0	2.47	−0.9	3.0
($\|c$)						2.55	−35.3	
Pr ($\|a$)	0.280	134	1.41[a]			3.67	−12.0	van Vleck's
($\|c$)						3.68	−23.7	paramagnetism
Nd ($\|a$)	0.286	138	1.36	101	3.3	3.59	−13.6	3.2
($\|c$)						3.69	−27.1	
Gd ($\|a$)	0.294	183	0.69	265	11.5	7.97	−11.0	11.5
($\|c$)						8.12	−15.6	
Dy ($\|a$)	0.282	59.4	0.276	215	1.4, 2.7	10.70	−5.6	3.5
($\|c$)						10.62	−12.1	

[a]Measured at 7.1 K.

$CeTe_2$.[11] The magnetic properties for the other $R\mathrm{Te}_2$ were recently reported by Shin *et al.* for $R=$Pr, Sm, and Gd,[12] where antiferromagnetic transition temperatures were found as low as 10 K for magnetic $R\mathrm{Te}_2$ except for $R=$Pr. A neutron-diffraction study on $CeTe_2$ (Ref. 13) exhibited that, below $T_N=4.3$ K, the magnetic moment orients along the stacking direction (crystallographic c axis) with the ferrimagnetic ground state. The precise magnetic measurements for $CeTe_2$ by Jung *et al.*,[14] however, revealed that the ground state is antiferromagnetic, and that a well-developed short-range order is present above the transition temperature associated with the low dimensionality of this magnetic system. In contrast to the intensive studies for $R\mathrm{Te}_2$, the physical properties of $R\mathrm{Te}_3$ have not been known, except for $SmTe_3$.

In this paper, we report on the magnetic behaviors of metallic $R\mathrm{Te}_3$ ($R=$Ce, Pr, Nd, Gd, and Dy) in comparison with those in $R\mathrm{Te}_2$ having a different conduction-carrier density. The difference of the magnetic anisotropy is manifested in these two compounds, although the symmetry at the R site is the same for both compounds. On the basis of the result, we propose designing magnetic structures in some composite layer compounds by the introduction of conducting carriers.

II. EXPERIMENT

Single crystals of $R\mathrm{Te}_3$ were prepared by a flux method using alkaline metal chloride according to DiMasi *et al.*[7] The mixture of the element powder with the total weight of 0.8 g was sealed in an evacuated quartz ample together with 1.6 g of the flux (LiCl:RbCl = 1:1). The ample was kept at 650 °C for two days. Then the temperature was gradually lowered to 540 °C in four days. The crystals had a reddish-yellow color and a metallic luster and were a rectangular shape with a size of up to $3\times3\times0.1$ mm^3. The lattice parameter in the stacking direction was measured by the x-ray powder-diffraction technique, and the in-plane structure was determined by a transmission x-ray Laue photograph using an imaging plate for the bulk crystals, and by electron diffraction for the cleaved fine crystals. All the lattice parameters were well coincident with those reported by DiMasi *et al.*[10] The distortion wave vectors Q associated with the formation of the superstructure are shown in the first column of Table I. The magnitude of Q is incommensurate with the in-plane lattice parameter and ranges from $0.27a^*$ to $0.29a^*$. The magnitude increases with the atomic number to $GdTe_3$, but sharply drops at $DyTe_3$. The condition of the superstructure formation is considerably different between the Gd and Dy compounds, such as the nesting condition of the Fermi surfaces as well as the lock-in effect to a commensurate value of the distortion wave vector. In any case, the difference of the Q vectors affects the size of the Fermi surfaces remaining after superstructure formation, giving significant difference in the electronic and transport properties.

The in-plane electrical resistivity of $R\mathrm{Te}_3$ was measured by a conventional four-probe method using gold wires as the electrical lead and gold paste as the conducting glue. When a kind of silver paste was used, the contact resistivity increased very rapidly. This fact indicates a chemical reaction such as a kind of intercalation reaction between the sample and glue. The temperature dependence of the resistivity was measured for $R=$La, Ce, Nd, Gd, and Dy down to 1.3 K.

The magnetic susceptibility and the magnetization curve of $R\mathrm{Te}_3$ were measured by a superconducting quantum interference device magnetometer between 300 and 1.8 K, with the magnetic field up to 5 T applied along the a and c axes. The magnetic susceptibility was fit to the Curie-Weiss law using the data above 200 K.

III. RESULTS

A. Electrical resistivity of $R\mathrm{Te}_3$

The electrical resistivity of $R\mathrm{Te}_3$ ($R=$La, Ce, Nd, Gd, Dy) was found to be metallic down to 1.3 K as shown in Fig.

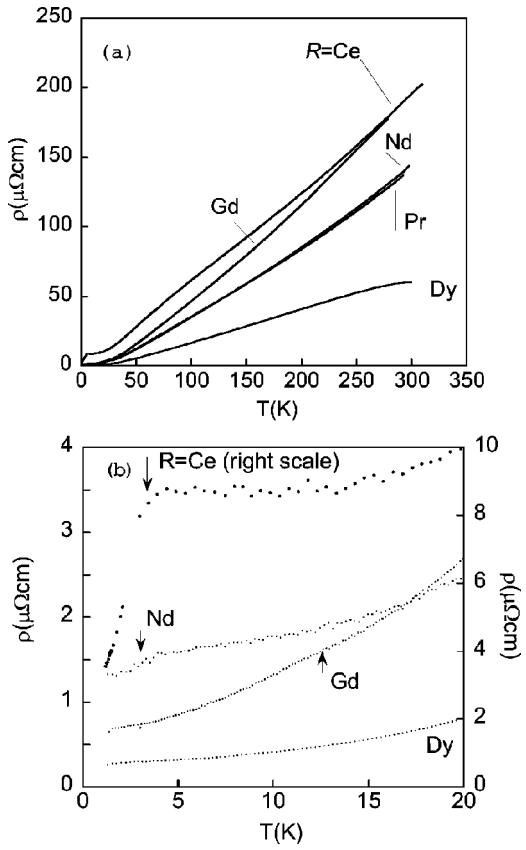

FIG. 2. (a) Temperature dependence of the electrical resitivity of $R\mathrm{Te}_3$ and (b) its low-temperature expansion. Arrows denote the anomalies associated with the magnetic transitions.

2, the behavior of which is the same as SmTe_3.[9] The room temperature resistivity and the residual resistivity at 1.5 K are summarized in Table I. The room-temperature resistivity ranged from 60 to 180 $\mu\Omega$ cm, and did not show regular dependence on the magnetic moment of the rare-earth element. The large room-temperature resistivity in CeTe_3 is due to the strong paramagnetic scattering because the localized Ce $4f$ level is relatively closer to the Fermi level than in other $R\mathrm{Te}_3$. The resistivity of DyTe_3 is about 1/3 that of GdTe_3, and is even smaller than the resistivity of nonmagnetic LaTe_3. This fact suggests that the significant difference of the electronic structure closely related to the carrier scattering is present between DyTe_3 and the other $R\mathrm{Te}_3$. The supersutructure formation makes the size of the Fermi surfaces and the conduction-carrier density reduced in comparison with those of undestorted $R\mathrm{Te}_3$ with a quarter-filled conduction band. As shown in Table I, the distortion wave vector Q of DyTe_3 is significantly different from those of $R\mathrm{Te}_3$, as mentioned in the preceding section. Presumably, the small room-temperature resistivity in DyTe_3 is attributed to the larger carrier density and the size of the Fermi surfaces after the superstructure formation.

The residual resistivity ratio (RRR) that equals $\rho_{rt}/\rho_{1.5\ \mathrm{K}}$ reaches up to 265 for GdTe_3. It is surprising that the residual resitivity ratio is so large despite the fact that the incommensurate lattice modulation due to the superstructure formation mentioned above exists in these compounds. This fact suggests that the lattice modulation is well ordered in the course of crystallization, due to the higher transition temperature of the lattice modulation than the temperature of the crystallization of $R\mathrm{Te}_3$. Since the residual resistivity is very low, the Shubnikov–de Haas oscillation in the magnetoresistance is found in LaTe_3 and CeTe_3 at lower temperatures. The results, including discussions of the electronic structures, will be reported elsewhere. As shown in Fig. 2 (b), weak anomalies of the resistivity were found for CeTe_3, NdTe_3, and GdTe_3 with decreasing temperature, as listed in Table I, suggesting the magnetic ordering in these compounds. The metallic behavior of $R\mathrm{Te}_3$ and the anomalies of the resistivity at the magnetic transition temperature suggest the presence of the RKKY-type interaction between the magnetic R atoms in contrast to semimetallic $R\mathrm{Te}_2$. However, this interaction is not significant in $R\mathrm{Te}_3$, except for CeTe_3, because the drop of the resistivity below the magnetic transition temperature as well as the magnitude of the paramagnetic scattering is quite small in $R\mathrm{Te}_3$.

B. Magnetic properties of CeTe_3

The temperature dependence of the magnetic susceptibility χ of CeTe_3 shown in Fig. 3(a) exhibits strong anisotropy due to the crystalline-field effect. The effective magnetic moments and the Weiss temperatures are obtained from the fit to the Curie-Weiss law to be $\mu_a = 2.47\mu_\mathrm{B}$ and $\theta_a = -0.9$ K when the magnetic field H is applied along the a direction, and $\mu_c = 2.55\mu_\mathrm{B}$ and $\theta_c = -35.3$ K for H applied along the c direction, respectively. The effective magnetic moments are close to the theoretical value of $2.54\mu_\mathrm{B}$ for the free Ce^{3+} ion. The susceptibility data are fit to a conventional crystalline-field model using Steven's operator. The point symmetry at the Ce site in CeTe_3 is C_4, so the Ce $4f$ states with the total angular momentum $J = 5/2$ split into following three Kramers:

$$|1\pm\rangle = \cos\theta|\pm 5/2\rangle + \sin\theta|\mp 3/2\rangle,$$

$$|2\pm\rangle = \sin\theta|\pm 5/2\rangle - \cos\theta|\mp 3/2\rangle,$$

$$|3\pm\rangle = |\pm 1/2\rangle.$$

As the anisotropy in χ is not so large at room temperature, the energy splitting between the ground and the highest exited states are supposed to be smaller than 300 K. Broad humps below 50 K in the inverse susceptibility versus the temperature curves are characteristic of the crystalline-field effect. Keeping these in mind, the susceptibility is fit to the crystalline-field model. The ground state is determined as $|1\pm\rangle = 0.54|\pm 5/2\rangle + 0.84|\mp 3/2\rangle$ and the energy splittings between the ground and the first exited state $|3\pm\rangle$ are estimated at 130 K, and that between the ground and the highest exited state $|2\pm\rangle = 0.84|\pm 5/2\rangle - 0.54|\mp 3/2\rangle$ at 230 K.

The magnetic susceptibility χ_a shows a small kink at 3.0 K, while no anomaly is found in χ_c. As shown in Fig. 2(b), the in-plane electrical resistivity of CeTe_3 shows a steep decrease below 3.0 K. Therefore, these anomalies in χ and ρ indicate a magnetic phase transition. The magnetization curve of CeTe_3 up to 5 T shows no anomalies and nearly

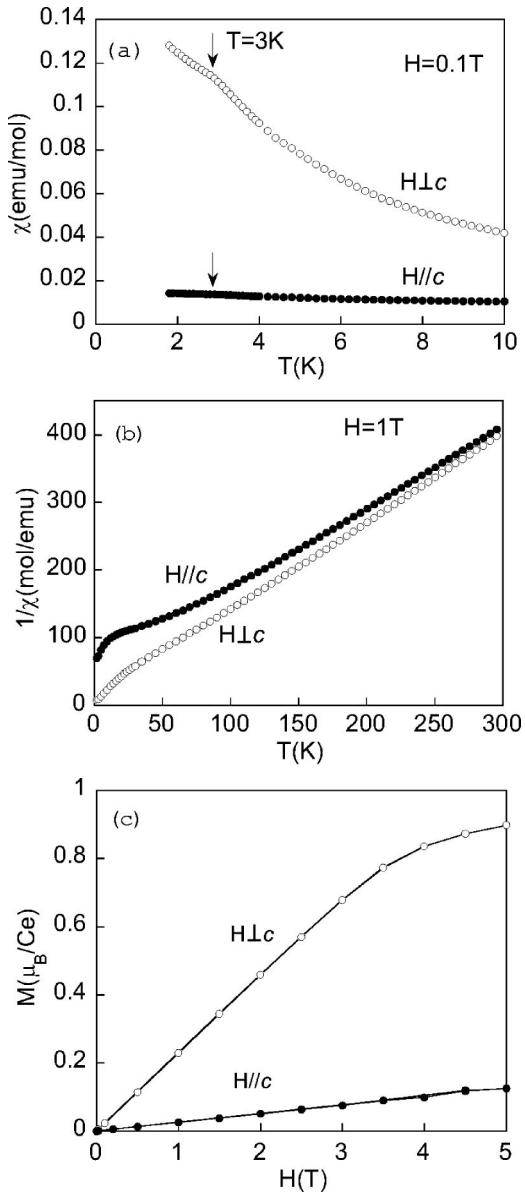

FIG. 3. (a) Magnetic susceptibility and (b) inverse magnetic susceptiblity of $CeTe_3$ as a function of temperature, and (c) magnetization curve of $CeTe_3$.

paramagnetic behavior [Fig. 3(c)]. When the magnetic field is applied perpendicular to the c axis, the magnetization almost saturates at 5 T with the saturation moment of $0.9\mu_B$/Ce. The moment is very close to the calculated moment of $g_J|\langle 1+|J_x|1-\rangle| = 0.87\mu_B$ for the ground state $|1\pm\rangle$. Since the anomaly in χ is very small, the magnetic transition is supposed to be not a simple antiferromagnetic transition, but a transition to a sort of helical or an incommensurate magnetic phase. In addition, the anomaly in ρ at 1.3 K suggests another magnetic transition at lower temperatures.

C. Magnetic properties of $PrTe_3$, $NdTe_3$, $GdTe_3$ and $DyTe_3$

The temperature dependence of the magnetic susceptibility and the inverse magnetic susceptibility, and the magnetization curves of $PrTe_3$ to $DyTe_3$ are shown in Figs. 4-7.

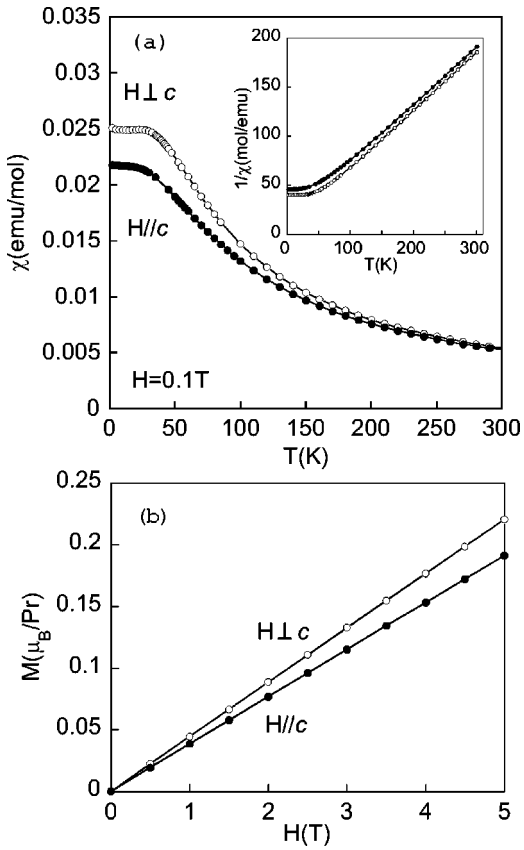

FIG. 4. Magnetic properties of $PrTe_3$. (a) Magnetic susceptibility at low temperatures, inset: inverse magnetic susceptibility as a function of temperature, (b) magnetization curve. Filled and open circles represent the magnetization for $H_{||}c$ and $H_{||}a$, respectively.

The magnetic susceptibility of $PrTe_3$ follows the Curie-Weiss law with $\mu_a = 3.67\mu_B$, $\theta_a = -12.6$ K, $\mu_c = 3.68\mu_B$, $\theta_c = -23.7$ K. μ_c and μ_a are close to $3.58\mu_B$ for Pr^{3+}. At lower temperatures than 100 K, the susceptibility deviates from the Curie-Weiss law and becomes nearly constant below 30 K. This behavior is typical for a magnetic system with the ground state being singlet. The magnetization curves show a straight line up to 5 T, where the magnetization is $0.22\mu_B$ for H_a and $0.19\mu_B$ for H_c.

The effective magnetic moments and the Weiss temperatures of $NdTe_3$ are obtained from the Curie-Weiss fitting, where $\mu_a = 3.59\mu_B$, $\theta_a = -13.6$ K, $\mu_c = 3.69\mu_B$, $\theta_c = -27.1$ K. At low temperatures, the magnetic susceptibility deviates from the Curie-Weiss law, and χ_c shows a broad maximum at 13 K. This is due to the crystal-field effect, and the fact that the ground-state $4f$ level has a small component of the magnetic moment along the c axis. However, χ_a shows a clear maximum at 3.2 K. At this temperature, χ_c also shows a weak anomaly. The magnetization curve for $H_{||}a$ taken at 1.8 K indicates a change of slope at around 3 T, as shown in Fig. 5(c). The magnetization at 5 T is only $1.4\mu_B$ for $H_{||}a$ and $0.1\mu_B$ for $H_{||}c$. Taking into consideration the anisotropic behaviors of the susceptibility and the magnetization curves, the ordered magnetic moment in $NdTe_3$ lies within the layer. It is also considered that another metamag-

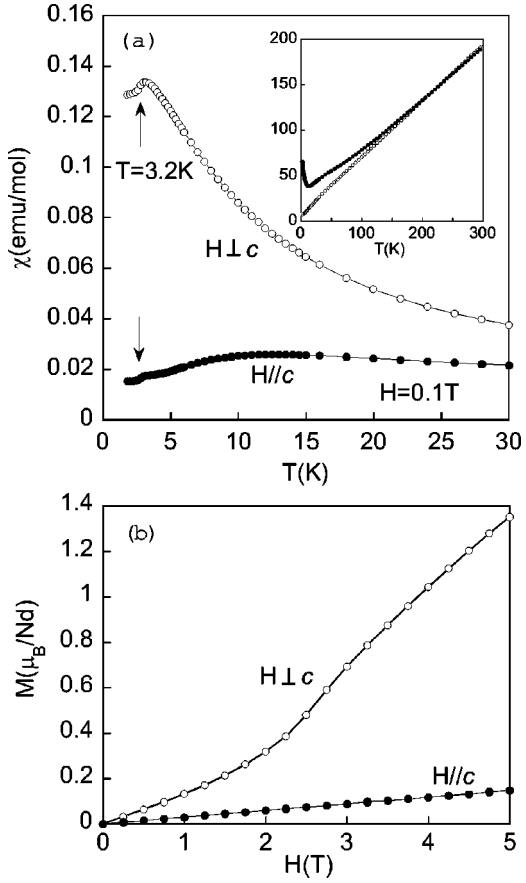

FIG. 5. Magnetic properties of $NdTe_3$.

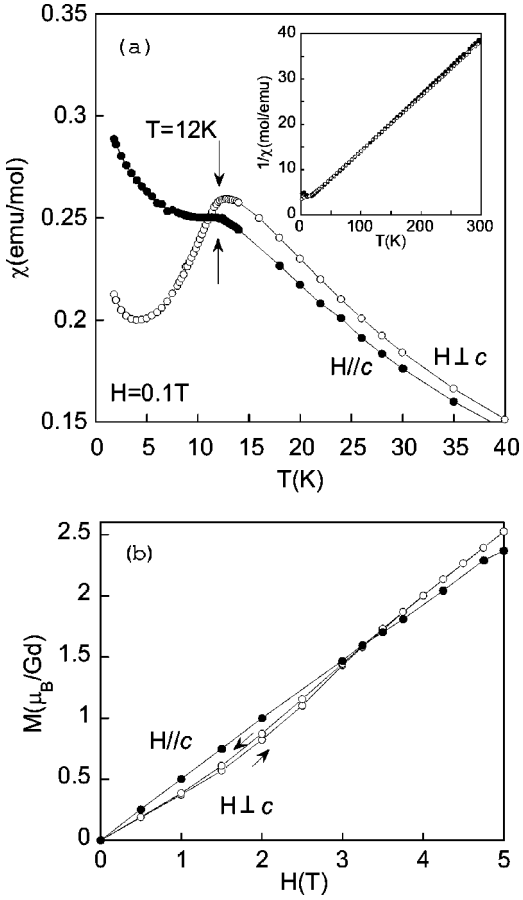

FIG. 6. Magnetic properties of $GdTe_3$.

netic transition may be present at a higher magnetic field because of the small magnetic moment in the easy axis at 5 T.

The magnetic susceptibility of the $GdTe_3$ at the paramagnetic region shows almost no anisotropy due to the half-filled $4f^7$ state with zero orbital angular momentum. However, as shown in Fig. 6(a), the anisotropy is present at and below 30 K. This feature is very similar to the behavior of $GdTe_2$,[12] and is common in the compounds having the GdX (X represents chalcogen) unit as known in $(GdS)_{1.20}NbS_2$.[15] The effective magnetic moment is $7.97\mu_B$, close to $7.94\mu_B$ for Gd^{3+}, and the Weiss temperature is -11.0 K. The temperature dependence of the susceptibility χ_a has a maximum at 11.5 K, which associates with an antiferromagnetic transition. The magnetization curve shows an anomaly when changing its slope at 2.5 T, suggesting a spin-flop transition.

The magnetic susceptibility of $DyTe_3$ shows different behaviors from those in other rare-earth tritellurides RTe_3. The effective magnetic moments and the Weiss temperatures are estimated at $\mu_c=10.70\mu_B$ and $\mu_c=10.62\mu_B$, very close to $10.63\mu_B$ of Dy^{3+}, and $\theta_a=-12.1$ K and $\theta_c=-5.6$ K. As shown in Fig. 6, χ_a is slightly larger than χ_c at low temperatures, and both show a maximum at 4.5 K and a steep decrease at 3.5 K. This behavior is typical for an antiferromagnet with the component of the ordered magnetic moments present both in the a and c directions. The magnetization curve for $H_{||}a$ shows metamagnetic transitions at 0.6 T and 0.9 T, and then shows a saturating behavior up to 5 T with the moment of $6\mu_B$/Dy. However, the magnetization for $H_{||}c$ shows two magnetic transitions at 0.9 T and 1.2 T, then the magnetic moment increases linearly and reaches $6\mu_B$ at 5 T. These behaviors imply the presence of many magnetic phases and a complicated M-H phase diagram below 5 T.

IV. DISCUSSION

First, we will discuss the magnetic anisotropy of RTe_3 in comparison with that in RTe_2. The common feature of the magnetic properties in RTe_3 is that the magnetic moment is perpendicular to the layer-stacking direction, except for the case of $DyTe_3$. This is in contrast to the magnetic anisotropy in RTe_2, where the magnetic moment lies parallel to the stacking direction. It is naturally considered that the magnetic anisotropy of these compounds is dominated by the crystalline-field effect, especially by the tetragonal crystalline-field parameter B_2^0 in this case. As can be seen in Fig. 1, RTe_2 and RTe_3 have a common basic structure, i.e., the alternate stacking of the RTe layer and the Te layer(s), so the coordination of Te atoms to an R atom is almost the same in RTe_3 and RTe_2. Therefore, the magnetic anisotropy also seems to be the same at first sight.

Taking the electron transfer from the RTe layer to the Te layer into consideration, however, the effective electric charge of Te in the Te layer becomes different. Figure 8 shows an illustration of the effective charge of Te around an

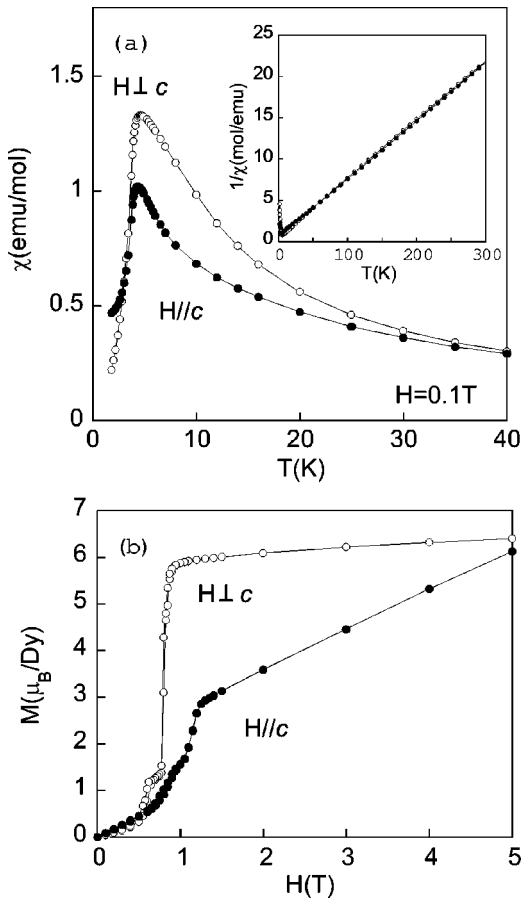

FIG. 7. Magnetic properties of $DyTe_3$.

R atom in RTe_2 and RTe_3, on the basis of one-electron transfer from the RTe layer to the Te layer(s). All the R-Te bond lengths are nearly the same with the value of about 3.3 Å. Therefore, the electric field at the R site yielded by four Te atoms in the Te layer can be roughly estimated as the field made by one Te atom hypothetically located in the tetragonal axis with the same R-Te atomic distance. In the case of RTe_3, the effective charge of the hypothetical Te atom is -1.0, while it is -2.0 for RTe_2, using the electric field being proportional to r^{-2}. Therefore, it can be considered that the electric crystalline field (CF) in RTe_2 is yielded from a distorted octahedron of six equivalent Te^{2-} ions. In contrast, in RTe_3, the reduced effective charge of Te in the Te layer gives a strongly anisotropic effect on the crystal electric field. This can vary the tetragonal CF parameter B_2^0 significantly, and cause the difference of the single-ion magnetic anisotropy in the $4f$ electrons of R.

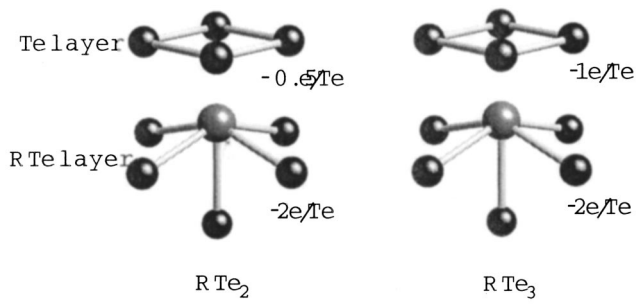

FIG. 8. Schematic illustration of the effective electric charge of the Te atoms that coordinate the R atom in RTe_2 and RTe_3.

These findings suggest that the magnetic structure as well as the magnetic anisotropy can be controlled by the introduction of an electric charge through the modification of the crystalline-field effect. It also should be noted that, in such layered compounds, the layer composite of the RTe_2 and RTe_3 units can produce designed magnetic structures with each magnetic moment perpendicularly ordered. Moreover, the direction of the ordered magnetic moment can be controlled by the introduction of other chemical species into the van der Waals gap of RTe_3 using the intercalation technique.

As shown in Table I, the effective magnetic moments estimated from the Curie-Weiss fitting at a higher-temperature region are well coincident with the effective moment of R^{3+}. It is known that this type of the compound shows nonstoichiometric composition with the deficiency of Te atoms, especially in RTe_2. However, as the magnetic measurements suggest, the chemical composition in the RTe_3 crystals is very close to the ratio of R:Te=1:3. This fact is also supported by the low in-plane residual resistivity, suggesting that almost no lattice defects or imperfections exist in the RTe_3 crystals.

The magnetic interaction in these compounds is more complicated than in RTe_2 because of the presence of conducting carriers. In the Gd compounds, the transition temperatures are known as 8.6 K for $GdTe_2$ and 11.5 K for $GdTe_3$, respectively. Since the $4f$ electron of the Gd atoms is not affected by the crystalline electric field, the magnetic anisotoropy and behaviors are very similar, and the contribution of the RKKY interaction and the effect of the interlayer separation can be directly compared in these two compounds. Although the increased interlayer distance between the magnetic layers in $GdTe_3$ weakens the interlayer magnetic interaction, the transition temperature of $GdTe_3$ is higher than that of $GdTe_2$. This implies that the conducting carrier plays a role in the magnetic interaction in this RTe_3 in addition to the dominant magnetic dipole interactions and the superexchange interaction through chalcogen atoms.

It is noted that the magnetic transition temperatures are lower in $CeTe_3$ than in RTe_2. By the single-ion anisotropy due to the crystalline field, the strong Ising-like behavior is expected for $CeTe_2$, while the XY-like behavior with a strong quantum fluctuation is expected for $CeTe_3$. It is natural that the increased degree of freedom in the XY system lowers the transition temperature. Therefore, although the RKKY interaction is much more important in $CeTe_3$ among RTe_3, the transition temperatures of $CeTe_3$ are possibly lower than those of RTe_2.

V. CONCLUSION

We have studied the magnetic properties of RTe_3 (R = Ce, Pr, Nd, Gd, Dy) by magnetization and electrical resistivity measurements, and found magnetic transitions at low temperatures. The higher magnetic transition temperature in conducting $GdTe_3$ than in $GdTe_2$ represents the role that the

conduction carrier also plays in magnetic interaction. On the other hand, the lower magnetic transition temperature in $CeTe_3$ than in $CeTe_2$ is attributed to the difference of the nature of their magnetic systems, XY-like for RTe_3 and Ising-like for RTe_2, originating from the single-ion anisotropy. The different single-ion anisotropy in RTe_3 and in RTe_2 is explained by the effective conduction-carrier density in the conducting Te layer. This result predicts that one can explore the different type of nanocomposite magnetic materials by introducing conducting carriers to the specific atomic layers. The candidates are, for example, R_mTe_n where $(m,n)=(2,5)$, $(3, 7)$, etc., where the structure consists of the alternate of the RTe_2 and RTe_3 unit. In these compounds, an independent magnetic order in each unit and perpendicularly ordered magnetic moments in different units can be expected.

[1] R. Wang, H. Steinfink, and W.F. Bradley, Inorg. Chem. **5**, 142 (1966).

[2] B.K. Norling and H. Steinfink, Inorg. Chem. **5**, 1488 (1966).

[3] M.P. Pardo, O. Gorochov, J. Flahaut, and L. Domange, Acad. Sci., Paris, C. R. **260**, 1666 (1965).

[4] A. Meetsma, G.A. Wiegers, R.J. Haange, and J.L. de Boer, Acta Crystallogr., Sect. A: Found. Crystallogr. **45**, 285 (1989).

[5] G.A. Wiegers, Prog. Solid State Chem. **24**, 1 (1996).

[6] A. Kikuchi, J. Phys. Soc. Jpn. **67**, 1308 (1998).

[7] E. DiMasi, B. Foran, M.C. Aronson, and S. Lee, Phys. Rev. B **54**, 13 587 (1996).

[8] A. Stowe, J. Solid State Chem. **149**, 155 (2000).

[9] E. DiMasi, B. Foran, M.C. Aronson, and S. Lee, Chem. Mater. **6**, 1867 (1994).

[10] E. DiMasi, M.C. Aronson, J.F. Mansfield, B. Foran, and S. Lee, Phys. Rev. B **52**, 14 516 (1995).

[11] Y.S. Kwon, T.S. Park, K.R. Lee, J.M. Kim, Y. Haga, and T. Suzuki, J. Magn. Magn. Mater. **140-144**, 1173 (1995).

[12] Y.S. Shin, S.W. Han, B.H. Min, H.J. Lee, C.H. Choi, Y.S. Kim, D.L. Kim and Y.S. Kwon, Physica B **291**, 225 (2000).

[13] J.G. Park, I.P. Swainson, W.J.L. Buyers, M.H. Jung, and Y.S. Kwon, Physica B **241-243**, 684 (1998).

[14] M.H. Jung, B.H. Min, Y.S. Kwon, I. Oguro, F. IGa, T. Fujita, T. Ekino, T. Kasuya, and T. Takabatake, J. Phys. Soc. Jpn. **69**, 937 (2000).

[15] O. Pena, P. Rabu, and A. Meerschaut, J. Phys.: Condens. Matter **3**, 9929 (1991).